



The atypical generation mechanism of Titan's Schumann resonance

Christian Béghin

► To cite this version:

Christian Béghin. The atypical generation mechanism of Titan's Schumann resonance. Journal of Geophysical Research. Planets, 2014, 119, pp.520-531. 10.1002/2013JE004569 . insu-01172663

HAL Id: insu-01172663

<https://hal-insu.archives-ouvertes.fr/insu-01172663>

Submitted on 7 Jul 2015

HAL is a multi-disciplinary open access archive for the deposit and dissemination of scientific research documents, whether they are published or not. The documents may come from teaching and research institutions in France or abroad, or from public or private research centers.

L'archive ouverte pluridisciplinaire **HAL**, est destinée au dépôt et à la diffusion de documents scientifiques de niveau recherche, publiés ou non, émanant des établissements d'enseignement et de recherche français ou étrangers, des laboratoires publics ou privés.

RESEARCH ARTICLE

10.1002/2013JE004569

Key Points:

- The parameters of Schumann cavity are constrained by the eigenmode equation
- ELF-modulated Pedersen current sheets are the sources of Schumann resonances
- Coupling mechanism between current-driven instabilities and QT whistler mode

Correspondence to:

C. Béghin,
christian.beghin@cnrs-orleans.fr

Citation:

Béghin, C. (2014), The atypical generation mechanism of Titan's Schumann resonance, *J. Geophys. Res. Planets*, 119, 520–531, doi:10.1002/2013JE004569.

Received 1 NOV 2013

Accepted 7 FEB 2014

Accepted article online 11 FEB 2014

Published online 11 MAR 2014

The atypical generation mechanism of Titan's Schumann resonance

Christian Béghin¹
¹LPC2E-CNRS-Orléans Université, Orléans, France

Abstract The observation of a presumed Schumann resonance (SR) during the landing of the Huygens Probe in Titan's atmosphere on January 2005 was subsequently reported and interpreted by Béghin et al. (2007, 2009, 2010, 2012) as being generated through the interaction of Saturn's magnetosphere with Titan's ionosphere rather than from the lightning activity that prevails on Earth. Beyond this atypical behavior, the existence of a single mode instead of the usual multimodal structure of terrestrial SRs and a comprehensive analysis of the physical generation mechanism remained to be investigated. The purpose of the present work is to draw up the baselines of a global model reconciling the Huygens data and the proposed generation mechanism. Based upon relevant observations obtained after several tenths of Titan's flybys by the Cassini orbiter, the modeling involves macro plasma physics processes as well as a global analysis of the mechanisms at the moon's scale. The clue to the SR's generation mechanism is shown to be the low-frequency modulation of the Pedersen current sheets that are induced in the ionopause region by the corotating Saturn's magnetosphere. The modulation principle involves a wave coupling between the ion-acoustic instabilities driven by the longitudinal current sheets and the electromagnetic quasi-transverse whistler mode. The spectral distribution of the sole second eigenmode seen by the Huygens Probe is found to comply with the ionopause plasma parameters measured by Cassini during the bipolar configuration of Titan-Saturn interaction that is thought to have occurred during the probe descent in the atmosphere.

1. Introduction

The sole extraterrestrial observation to date of a most likely Schumann resonance phenomenon was made on board of the Huygens Probe that landed on Titan's surface in January 2005. Extremely low frequency (ELF) waves were detected by the HASI-PWA (Huygens Atmospheric Structure, Permittivity, Wave, and Altimetry Instrumentation), in the same time as measurements of electron and ion atmospheric conductivities [Fulchignoni et al., 2005; Grard et al., 2006]. The fact that only the second eigenmode of the Titan's Schumann resonance (SR) be visible in ELF-PWA data was pointed out in a preview work [Béghin et al., 2007]. Numerical simulation showed that the amplitude spectral distribution (ASD) of the electric field components of usual SR eigenmodes might be explained by the angular separation between the observer site and a supposedly monopole point source [Simões et al., 2007]. In the simulation, the source was lying in the atmosphere at an altitude of 35 km above a subsurface dielectric layer of thickness $z_c = 100$ km with a permittivity $\epsilon_c = 3$, overlapping a perfectly conductive surface. For a source-observer separation of 90° , the signal of the fundamental mode at around 20 Hz was found to lie near a node location, about 3 times weaker than the second one at 36 Hz, and slightly depending on the altitude of the observer. In the same conditions, the higher eigenmode orders were found progressively being more and more damped, which is consistent with Earth's SR observations. Besides, another phenomenon known on Earth could also lead to a dependence upon the source-observer longitudinal separation. This is the mode-splitting phenomenon [Nickolaenko and Sentman, 2007], due to interferences between a main stationary eigenmode and two tesseral modes of the same degree. These modes are progressive waves propagating in opposite directions with respect to the source location, assuming a homogeneous spherical cavity. Such effects are not relevant here, essentially because the assumption of localized vertical current sources is no more valid after the recognized absence of lightning activity in Titan's atmosphere [Fischer and Gurnett, 2011]. Therefore, the tesseral Longitudinal Section Magnetic (LSM) modes were proposed to be associated with longitudinal ELF current sources induced in the upper ionosphere by the corotating Saturn's magnetosphere [Béghin et al., 2012]. These modes are known indeed to be the only ones able to be excited by current sheets lying at the upper bound of

spherical cavities [e.g., Wait, 1962; Galejs, 1972; Collin, 1991]. The different steps of the approach described in this article are successively developed in the following sections.

In section 2, starting from the SR modal equation derived from the physical characteristics of a multilayered spherical cavity [Béghin et al., 2012], the theoretical ASD composite response of the two first SR modes added to the instrumental noise is compared with the PWA data. The same operation is subsequently performed with the second mode combined with the third one. Then, the demonstration being made that no signature of any mode beyond 42 Hz might be visible in the data, the possibility that the observed signals be generated within a bounded frequency range is investigated in section 3. According to a primary suggestion by Béghin et al. [2012], a first attempt aims to explain the absence of higher modes due to the natural cutoff frequency of the current-driven ion-acoustic instability, namely, the ion-plasma frequency. For that purpose, a standard model of plasma parameters of the ionopause region is derived, based upon the Cassini observations performed in the daylight hemisphere during a situation of bipolar configuration of the ramside Saturn's magnetic field lines [Simon et al., 2013]. Such situation is assumed to be applicable to the Huygens descent in the atmosphere. After the ion-plasma cutoff frequency being revealed to lie well above the higher frequency of PWA ELF data, the wave-coupling mechanism between the current-driven ion-acoustic instabilities and the QT whistler mode, initially proposed by Béghin et al. [2007], is revisited in section 4 in the framework of a current sheets modulation mechanism.

2. Comparison Between the Theoretical ASD Responses and the PWA Data

The mathematical developments presented in this paper are derived from previous works, and more specifically in Béghin et al. [2012] as regards the SR modal equations in a longitudinally multilayered spherical cavity, which read

$$\omega_l = \frac{c}{a} \left[l(l+1) \frac{h_1 + z_c / \text{Re}(\epsilon_c)}{h_2 + z_c} \right]^{1/2} \left[1 - i \left(\frac{z_c \delta / \text{Re}(\epsilon_c) + \pi \zeta / 4}{h_1 + z_c / \text{Re}(\epsilon_c)} + \frac{\pi \zeta / 4}{h_2 + z_c} \right) \right] \quad (1a)$$

$$Q_l = \frac{|\text{Re}(f_l)|}{2 |\text{Im}(f_l)|} = \left[\frac{2 z_c \delta / \text{Re}(\epsilon_c) + \pi \zeta / 2}{h_1 + z_c / \text{Re}(\epsilon_c)} + \frac{\pi \zeta / 2}{h_2 + z_c} \right]^{-1}, \quad (1b)$$

where $\omega_l = 2\pi f_l$ is the complex angular frequency for any eigenmode of degree l and Q_l is the associated quality factor (a real quantity); c is the free-space light velocity and a the Titan's mean radius (~ 2575 km), h_1 and h_2 are the altitudes of the conduction and diffusion bounds, respectively, within the atmospheric portion of the cavity, ζ is the average-scale height of the electron conductivity from h_1 up to h_2 , assuming a smoothed exponential law in between, and z_c , ϵ_c , and δ are the thickness, permittivity, and loss tangent, respectively, of the Titan's surface icy crust. The symbols Re and Im are used for real and imaginary part of the quantities. The local amplitude of the radial electric field component E_r of any LSM_l^m eigenmode of order m and degree l , with the frequency f_l , trapped inside a layered spherical cavity, is derived from Maxwell's equations in terms of a scalar potential [Béghin et al., 2012] as

$$|E_r| = \frac{\text{Re}(\omega_l) l(l+1)}{k^2 a^2} \frac{A_r}{n^2} Y_l^m(\theta, \varphi) \approx C^{\text{te}} \frac{l(l+1)}{f_l} Y_l^1(\theta, \varphi), \quad (2)$$

where A_r is the amplitude of the radial Hertzian potential [Collin, 1991], n is the local value of index of refraction, and k the wave number. Note that in the derivation of the last term of equation (2), the basic relation $k^2 n^2 c^2 = \omega_l^2$ is used. $Y_l^1(\theta, \varphi)$ is the first order spherical harmonic function associated with the relative coordinates between the source and the Huygens landing site, which reads

$$Y_1^1 = -\sin\theta \cos\varphi; Y_2^1 = \frac{3}{2} \sin 2\theta \cos\varphi; \text{ and } Y_3^1 = \frac{3}{2} \sin\theta (1 - 5 \cos^2\theta) \cos\varphi, \quad (3)$$

where θ and φ are the differential latitude and longitude, respectively, between Huygens and the most efficient portion of the main current source. As long as we are interested in the amplitude ratio between the radial components of the two first modes, applying equations (2) and (3), after canceling all constant quantities, yields

$$\frac{|E_2|_{\text{max}}}{|E_1|_{\text{max}}} = 9 \frac{f_1}{f_2} \cos\theta. \quad (4)$$

Although the landing site latitude is known (about 10°S), the ramside location of the upstream current sources associated with the induced magnetotail on 14 January 2005 might be only speculative. However,

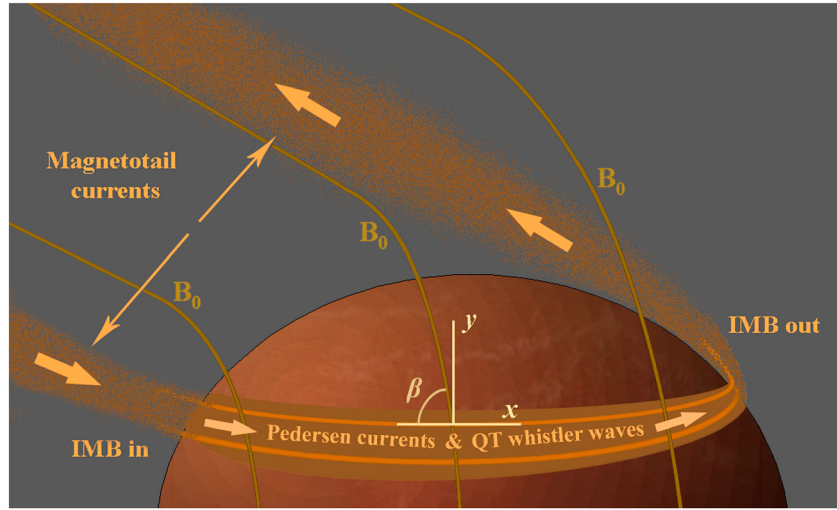


Figure 1. Sketch of draped Saturn's magnetic field lines in northern Titan's ramside hemisphere and the induced longitudinal Pedersen current sheets. The reconnection mechanism between the magnetotail field-aligned currents and the ionospheric currents is similar to that one seen between the Earth's *E* layer electrojet and the auroral field-aligned currents.

the northern and southern latitudes of draping field lobes of magnetotail currents (Figure 1) were observed during Titan flybys T B and T3 by the Cassini orbiter about 1 month before and after Huygens landing. For each of both flybys, either of both lobes was seen in a bipolar configuration [Simon *et al.*, 2013], i.e., lying symmetrically with respect to the Titan's orbital plane. In that lapse of time there was no major solar wind evolution, neither any significant seasonal evolution of Titan-Saturn configuration. One may then reasonably assume that the Huygens landing site was located between 20 and 60° latitude apart from either of northern-southern upstream ionospheric currents.

Assigning to each mode the same SR cavity parameters as those deduced from the spectral characteristics of the observed second mode, the frequency ratio between the two first modes is fully determined by equation (1a) and the cavity parameters, such as

$$3 \left| \frac{f_1}{f_2} \right|^2 = \left(\frac{h_1(f_2) + \zeta \ln(f_1/f_2) + z_c / \text{Re}(\epsilon_c)}{h_2(f_2) - \zeta \ln(f_1/f_2) + z_c} \right) \left(\frac{h_2(f_2) + z_c}{h_1(f_2) + z_c / \text{Re}(\epsilon_c)} \right). \quad (5)$$

An analytic approximation of the ASD response of the cavity for each individual mode may be predicted using the Laplace transform [Bateman and Erdelyi, 1954] applied to passive linear networks excited by a Dirac source current, which reads

$$E_l(t) = C^{\text{te}} \exp - \left[\frac{1}{2Q_l} + i \right] \text{Re}(\omega_l) t \xrightarrow{\text{LT}} G_l(\omega) = C^{\text{te}} \frac{i}{\omega - \text{Re}(\omega_l) + i \text{Re}(\omega_l) / 2Q_l}. \quad (6)$$

Thus, if $f_l = \text{Re}(\omega_l) / 2\pi$ is the peak frequency of a mode of degree l , the normalized frequency response of $E_l(f)$ versus the peak value E_{Max} derived from equation (6) reads

$$\frac{E_l(f)}{E_{\text{Max}}} = \left(1 + 4Q_l^2 (1 - f/f_l)^2 \right)^{-1/2} e^{i\psi} \text{ and } \psi_l(f) = \text{atan} \frac{1}{2Q_l(f/f_l - 1)}, 0 < \psi_l < \pi, \quad (7)$$

where $E_l(f)$ and ψ_l are the amplitude and the phase, respectively, of the ASD complex function of the considered mode. Therefore, the composite signal of the two first modes alone (without the instrumental noise) is the addition of two coherent vectors in the complex plane, which reads

$$E_{12}(f) = (|E_1|^2 + |E_2|^2 + 2|E_1 E_2| \cos(\psi_1 - \psi_2))^{1/2} \exp(i\psi_{12}), \quad (8a)$$

$$\psi_{12} = \text{atan} \frac{|E_1| \sin \psi_1 + |E_2| \sin \psi_2}{|E_1| \cos \psi_1 + |E_2| \cos \psi_2}. \quad (8b)$$

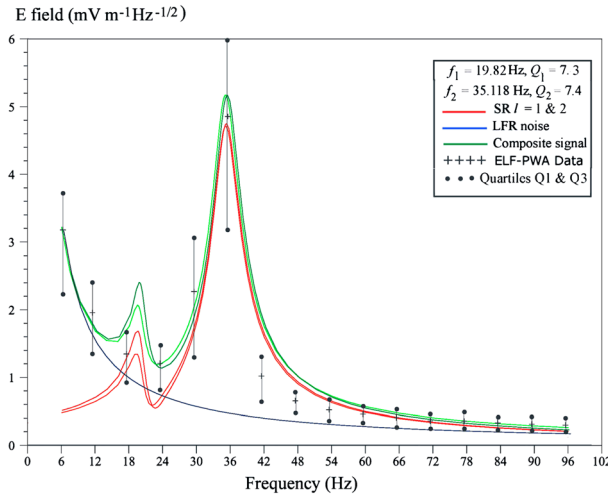


Figure 2. Case study # 1 simulation of the two first SR modes. The couples of red and green curves are for $\theta = 20^\circ$ and 40° , respectively. Note that the presence of the first mode would have more than a 50% probability to be compatible with the 24 Hz bin PWA data, whereas the probability is less than 25% for the bin 18 Hz.

The normalization of the computed electric field values with respect to the experimental data, is obtained using the ADS average of a PWA sequence of 232 spectra, made of the odd 16 bins from 6 to 96 Hz with 3 Hz resolution, and performed between 108 and 72 km of altitude when the signal reached its maximum strength [Béghin *et al.*, 2007]. The averages of both measured ADS values of bins 30 and 36 Hz are taken as a reference for the normalization of the theoretical response of the second mode. Introducing in equation (7) the two quantities $|E_2(30)|$ and $|E_2(36)|$, after ruled out E_{Max} yields

$$\frac{1 - B_2^2}{4Q_2^2} + \left[1 - \frac{36}{f_2}\right]^2 - B_2^2 \left[1 - \frac{30}{f_2}\right]^2 = 0, \quad (9)$$

with $B_2 = \frac{|E_2(30)|}{|E_2(36)|}$.

One obtains then two independent quantities, namely, Q_2 and f_2 that are cross constrained

through equations (8) and (9) independently from E_{Max} and the latter is determined furthermore using equation (7).

Two case studies, selected among the cross-constrained values of f_2 , Q_2 , and $|E_2|_{\text{Max}}$, have been considered (Table 1), with their own cavity parameters relevant to each particular case.

Assuming, first, that the ASD analytic expression of the instrumental noise may be represented by a linear flicker regression (LFR) law representing the spectral distribution of noise in semiconductor devices [e.g., Leach, 1994, and references therein] and second, that the nature of PWA data at the lowest and highest frequencies is essentially of that kind, the noise contribution obeys the following LFR function (solid blue curve plotted in Figures 2 and 3)

$$\text{LFR}(f) = A/f^\alpha, \quad (10)$$

where $A = 21.945 \text{ mV m}^{-1} \text{ Hz}^\alpha$ and $\alpha = 1.08544$ are the two coefficients deduced from a least squares regression analysis of a two columns matrix made of the 246 spectra of the 140–110 km sequence (ignoring the 36 Hz bin), when the amplitude of the signal is very weak [Béghin *et al.*, 2007]. Thereafter, the complex computed ASD sum of two first modes (equations (8a) and (8b)) is added to the noise function according a similar procedure, with a mean LFR phase value of noise, $\psi_n = \alpha \pi/2$. The resulting combined spectral responses for the case study # 1 are plotted in Figure 2 for the two first modes only (solid red lines), then with the noise added (solid green lines) for comparison with the PWA data (black crosses).

One can see that the statistical dispersion of the PWA data, namely, the average ASD values plus-minus the two quartiles Q_1 and Q_3 (black dots) are overlapping symmetrically the simulated responses of both modes at bins 24, 30, and 36 Hz, but marginally at the bin 18 Hz. The quartiles are preferred here to the traditional standard deviation for quantifying the dispersion of the values. The reason is because the amplitude fluctuations of the electric field component seen by the dipole antenna are not randomly distributed, as they depend essentially on the quasiperiodic tilt and spin motions of the Huygens Probe [Béghin *et al.*, 2009]. Since

Table 1. Parameters for Case Study Simulations of the Three First Eigenmodes Constrained by Equations (1a)–(9)

Parameters (Unit)	f_l (Hz)	Q_l	h_1 (km)	σ_1 (S m^{-1})	h_2 (km)	σ_2 (S m^{-1})	ζ (km)	z_c (km)	ε_c	δ	θ (deg)	E_{Max} ($\text{mV m}^{-1} \text{ Hz}^{-1/2}$)
Case # 1	$l=2$	35.118	7.4	1.95×10^{-9}	172	1.9×10^{-5}	6.9	60	2	2.4×10^{-2}	20–40	4.73
	$l=1$	19.82	7.3	1.1×10^{-9}	176	3.36×10^{-5}	id.	id.	id.	id.	id.	0.99–1.215
	$l=3$	49	7.46	2.73×10^{-9}	170	1.38×10^{-5}	id.	id.	id.	id.	60	1.69
Case # 2	$l=2$	36.1	5.9	2.0×10^{-9}	157	3×10^{-5}	5.4	80	1.8	0.129	40–60	4.415
	$l=1$	20.5	5.83	1.14×10^{-9}	160	5.3×10^{-5}	id.	id.	id.	id.	id.	1.13–1.73
	$l=3$	50.5	5.95	2.8×10^{-9}	155	2.16×10^{-5}	id.	id.	id.	id.	60–64	1.58–0.28

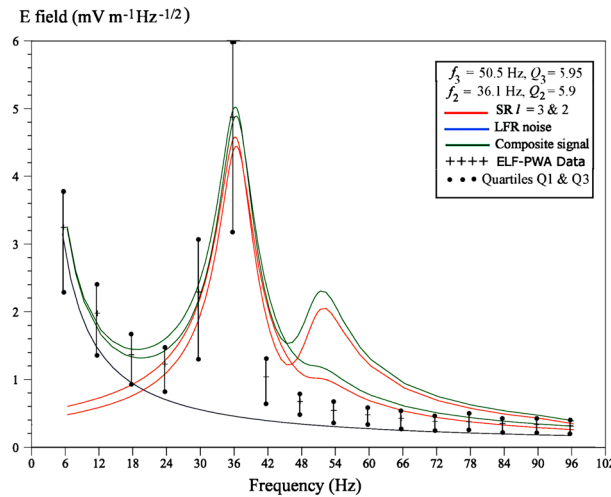


Figure 3. Same as Figure 2 for case study # 2. The couples of red and green curves are for $\theta = 60^\circ$ and 64° , respectively. For $\theta = 63 \pm 1^\circ$, the presence of the third mode would be marginally visible in bin 54 Hz.

the presence of the third mode should have been visible in the PWA data whatever the value of θ , except for two unlikely descent trajectories of Huygens, i.e., $\theta = 0^\circ$ and $\sim 63.4^\circ$ with respect to the current sources. Therefore, we will consider from now on the existence of an upper cutoff frequency at around 40–50 Hz in the generation mechanism, the first one of which might be the ion-plasma frequency, i.e., the upper limit of the current-driven ion-acoustic instability presumed to be present in the source region.

3. Modeling of Induced Current Sheets in the Ionopause Region

The current-driven ion-acoustic instability [e.g., Alexandrov *et al.*, 1984] was considered as a substitute for the source of SR in the absence of lightning activity in Titan's atmosphere [Béghin *et al.*, 2007], and the same instability has been proposed to explain the escape of negative ions above the Titan's ionopause [Rosenberg and Shukla, 2009]. The upper bound of the ELF range covered by this instability is the minimum local value of the ion-plasma frequency (f_{pi}), which obeys the relation

$$f_{pi} = \frac{|q_i|Z}{2\pi} \left(\frac{n_i}{m_i \epsilon_0} \right)^{1/2}, \quad (11)$$

where n_i is the positive ion density assumed to be at least the same as n_e ; here $Z = 1$, i.e., the minimum ionization state of ions, then $|q_i| = q_e$, and m_i is the mean mass of positive ions. The first idea consists to postulate [Béghin *et al.*, 2012] that the minimum value of f_{pi} in the source region would lie at about 40–50 Hz, such as then no higher SR modes would be excited. After a preliminary survey of a few Titan's flybys by Cassini, it appears that the ELF spectrum of the electric field components observed by the Radio and Plasma Wave Science (RPWS) instrument [Gurnett *et al.*, 2004] onboard the Cassini orbiter may exhibit indeed a cutoff at around 40–60 Hz, as for instance during the flyby # T5 on 16 April 2005 (Figure 4), while crossing the northern or southern lobes of the Induced Magnetospheric Boundary (IMB). Though the frequency range is compatible with that of possible SR eigenmodes, the nature of ELF waves observed on board Cassini at the altitude of the IMB's (~ 2500 km in T5 case) could not be formally proven to be related with the ionopause current sheets. However, with the opportunity of several Cassini closest approaches (CA) as low as 1050–950 km from the surface, the existence of multilayered current systems have been revealed at such altitudes [Ågren *et al.*, 2011]. These two positive facts bring significant material for updating the investigation of the generation mechanisms of Titan's Schumann resonances in the ionopause region.

3.1. Structure and Composition of the Ionopause Region Applicable to Huygens Descent Conditions

A noticeable point, visible in Figure 4, is that the stronger electric field components are seen during both IMB crossings, while the magnetic wave components do not emerge from the instrumental noise throughout the flyby pass. It is worth to recall that the IMBs, also named draping boundaries [Neubauer *et al.*, 2006], might be defined as the inbound and outbound connection spots between the magnetotail current lobes and the

Q_1 and Q_3 are splitting, respectively, the lowest 25% and 75% fractions of the data series, the fact that the composite values of the bin 24 Hz are lying between these bounds implies at least a 50% probability that the presence of a first mode be compatible with the PWA data when $\theta = 20^\circ$. However, the presence of the first mode does not comply with more than a 25% probability to appear in the bin 18 Hz. It must be also noted that if θ would be nearly zero, which is a node location according to (equation (3)), all three modes would be totally absent in PWA data.

A similar procedure was applied to the combination of modes 2 and 3, plus the noise in the case study # 2 (Figure 3).

According to the expression of Y_3^{-1} (equation (3)), one can see that the

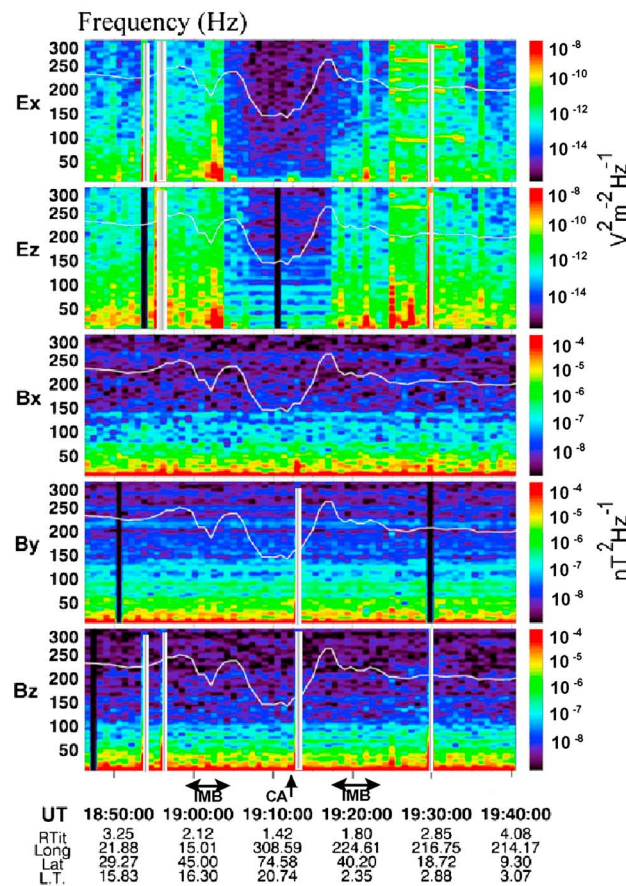


Figure 4. ELF wave spectrogram of Titan's flyby # T5 with closest approach 1050 km above the surface, measured by the RPWS instrument [Gurnett *et al.*, 2004]. The white line is the local value of electron cyclotron frequency f_{ce} (excerpt from Béghin *et al.* [2009], with permission from Elsevier).

lying roughly below 1200 km, as it appears marked as a sharp decrease of the amplitude B_0 of the magnetic field. This fact is visible in Figure 4 by the sudden decay of the electron cyclotron frequency from about 260 to 140 Hz, i.e., B_0 from 9.3 to 5 nT. The following standard model of vertical profiles of physical parameters of Titan's ionopause region is built by referring as far as possible to the average data collected by the Cassini orbiter during low CA flybys over the ramside daylight hemisphere performed a few years after Huygens landing. Note that a recent survey of plasma parameters measured with the Langmuir Probe of RPWS experiment during 52 Titan's flybys [Edberg *et al.*, 2010] confirms substantially the model presented below. Since the Huygens descent was accomplished during quiet solar activity, a nominal bipolar configuration [Simon *et al.*, 2013] is assumed to be applicable. Then, the primary magnetic field lines induced by Saturn's magnetosphere are thought to be draped around the ramside upper ionosphere [Neubauer *et al.*, 2006], with a nominal dip angle of $90^\circ \pm 15^\circ$ with respect to the presumed latitudinal orientation of the current sheets (Figure 1). For purpose of simplicity, one considers a one-dimensional model in which all varying parameters are supposed to be functions of the altitude (z) only.

The derivation of the main parameters obeys different assumptions, as described below:

1. The first relevant parameter is the altitude profile of the magnetic field which is assumed obeying the MHD balance between the magnetic pressure $p_{mag} = B_0^2/2\mu_0$ and the thermal pressure p_{th} [Keller *et al.*, 1994], starting from $B_0 = 10$ nT in the undisturbed regions assumed to lie at about 1.5 Titan's radii (~ 1300 km above the surface). The thermal pressure is derived from HASI data [Fulchignoni *et al.*, 2005], and B_0 is slowly decreasing down to the equality of both pressures at 1130 km (Figure 5). Thereafter, B_0 vanishes exponentially with a scale height of 100 km, and small irregularities are considered down to 1030 km (Figure 5). The geographic inclination β (dip angle) of the magnetic field vector \mathbf{B}_0 with respect to the longitudinal axis X (Figure 1) is given three possible values (85° , 80° , and 75°) corresponding to deviations around a purely bipolar configuration.

induced ionospheric sheets of currents (Figure 1). This fact supports the idea that the ion-acoustic electrostatic waves might be generated at lower altitudes than the IMBs and be transported upward along the current lines. The question now is to identify where the ion-acoustic instability may reach its maximum of efficiency, and in which frequency range.

For this purpose, let us consider first the most likely model of Titan's ramside upper ionosphere in daylight conditions that could be relevant to the Huygens descent. The region of maximum strength of the induced currents is predicted by MHD models [e.g., Keller *et al.*, 1994] to lie in the vicinity of the ionopause. The latter is defined as the boundary where the thermal pressure is balanced by the incoming Saturn's magnetosphere pressure, so as the magnetic field is dissipated at lower altitude faster than it can be replenished from the upper ionosphere [Keller *et al.*, 1994]. In this region, the currents obey the generalized Ohm's law $\mathbf{J} = \sigma \mathbf{E}$, where σ is the tensor of conductivity [e.g., Baker and Martyn, 1953] and \mathbf{E} is the dynamo electric field induced by the Saturn's corotating magnetosphere. After examination of several Titan's flybys with low-altitude CA, the lower bound of the dynamo region may be estimated

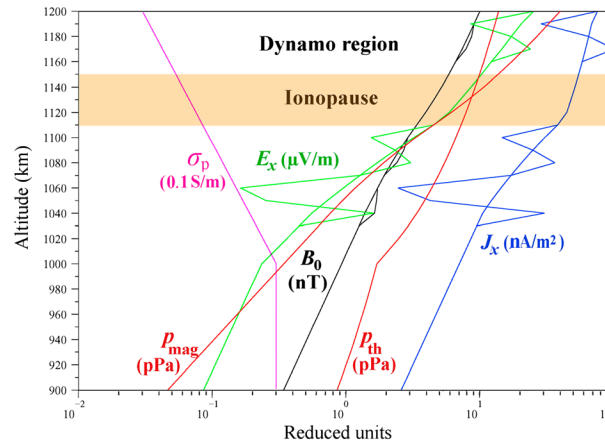


Figure 5. Distribution of physical parameters in Titan's ramside upper ionosphere applicable to the conditions of the Huygens descent. Note that small-scale amplitude variations of B_0 yield strong layering of longitudinal current sheets and associated electric field. The ionopause is marked by the balance between both magnetic and thermal pressures occurring at ~ 1130 km.

conditions measured by the Cassini radio occultation experiment [Kliore et al., 2008], in agreement with Cassini routine measurements in the same conditions [Wahlund et al., 2009]. The minimum positive ion density n_i is assumed to be equal to n_e .

5. As a first approximation, the ion temperature is assumed to be everywhere that of the neutral gas, and the electron temperature T_e is given a reference value of 1000 K at 1200 km (Figure 6). The electron temperature profile is an average of Cassini flybys measurements between 1200 and 1000 km [Galand et al., 2006] and deduced from MHD model [Keller et al., 1994] below 1000 km, as well as the thermal pressure $p_{th} \sim n_e K_B T_e$, where K_B is the Boltzmann constant (1.38×10^{-23} J/K). Below 1000 km p_{th} is given a regular decay down to 900 km (Figure 5), assuming that the thermalization of the plasma (i.e., $T_e = T_i = T_n$) is fully achieved in that region, as shown in Figure 6.

At the altitudes higher than the ionopause, the magnetic pressure is larger than the thermal pressure, and the vertical gradient of B_0 increases progressively in the dynamo region (Figure 5). Within a wide range of altitudes, on both sides of the ionopause, the longitudinal current sheets J_x are generated in virtue of Maxwell-Ampère's law

$$\mathbf{J} = \frac{\text{curl}(\mathbf{B}_0)}{\mu_0} \Rightarrow J_x = \frac{1}{\mu_0} \frac{\partial B_0}{\partial z}, \quad (12)$$

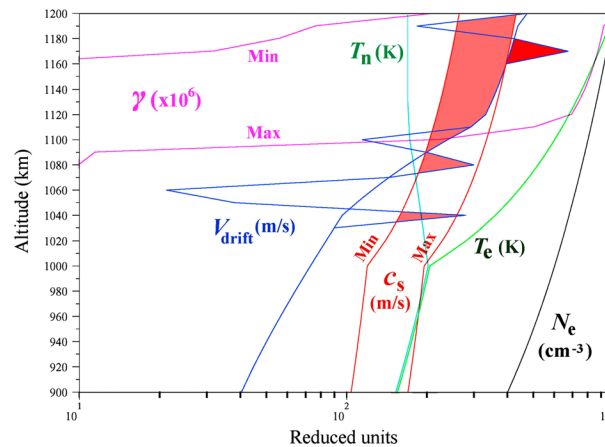


Figure 6. Vertical profile of parameters controlling the ion-acoustic instability. Note the layering structures of V_{drift} overlapping the smooth profiles of J_x and E_x associated with the irregularities of B_0 plotted in Figure 5.

2. Since we are mainly concerned with the upper limit of the ion-acoustic instability, one considers low life duration complex species which ultimately convert into higher-mass ions such as HCNH^+ and C_3H_5^+ through dissociative recombination reactions producing extremely heavy ions (ranging from $m_i = 45$ up to 120 amu), as reported from Cassini observations [Crary et al., 2009].
3. The altitude profiles of neutral gas density—essentially nitrogen—and temperature T_n are derived from HASI measurements [Fulchignoni et al., 2005]. The density profile of n_n is given a normalized value of 10^{10} cm^{-3} at the altitude of 1000 km [Cui et al., 2009] with a scale height of 62.5 km.
4. The profile of electron density n_e is the average between dusk and dawn

in which the invariability of longitudinal and latitudinal components of B_0 is assumed in this model. In these conditions, the longitudinal currents J_x are essentially supported by the Pedersen conductivity σ_p (Figure 1). The altitude profiles of the three components of conductivity in the dynamo region have been derived from in situ measurements, using the Langmuir Probe and the Magnetometer instruments during the Cassini flybys [Rosenqvist et al., 2009], from where a smoothed average profile of the Pedersen conductivity is considered here (Figure 5). Using the expression of J_x given in equation (12), one obtains an estimate of the longitudinal electric field amplitude $E_x = J_x / \sigma_p$ plotted together with

σ_p and J_x in Figure 5. Note that superposed to their smoothed profiles, the quantities E_x and J_x exhibit strong localized irregularities of amplitude due to natural variations of \mathbf{B}_0 , the vertical gradient of which induces large variations of J_x according to equation (12). The latter phenomenon is thought to be the cause of the layered structure of the thin longitudinal current sheets derived from data of the Cassini plasma and wave sciences instruments [Ågren *et al.*, 2011].

3.2. Induced Longitudinal Current Sheets and Current-Driven Ion-Acoustic Instability

The specific criterion for triggering the ion sound waves is when the electron-ion drift velocity V_{drift} exceeds the adiabatic ion-acoustic speed c_s , which reads

$$V_{\text{drift}} \geq c_s, \text{ i.e., } V_{\text{drift}} = \frac{J_x}{n_e q_e} \geq \left(\frac{K_B T_e}{m_i} \right)^{1/2}. \quad (13)$$

Nevertheless, the parameters of the model proposed in the previous section controlling the current strength (J_x), and the ion-acoustic instability are subject to significant dispersion, the latter being essentially due to several factors such as, (i) the vertical profile of B_0 and its variations, (ii) the wide range of ion mass (45–120 amu), and (iii) the difference between dusk-dawn profiles of n_e . Substituting in equation (13), the altitude profiles of J_x , n_e , T_e , and min-max values of m_i allows us to identify the region where the ion-acoustic instability may occur more likely (Figure 6, highlighted area).

The kinetic dispersion equation of the ion-acoustic instability [e.g., Alexandrov *et al.*, 1984], with wave harmonic amplitudes in form of $\exp[i(k_{ia} - \omega_{ia}t)]$, generated by an electron-ion drift velocity (V_{drift}), yields the following solution for real and imaginary parts of the ion-acoustic frequency

$$\text{Re}(\omega_{ia}) \approx k_{ia} c_s \quad \text{with} \quad c_s = \sqrt{\frac{K_B T_e}{m_i}}, \quad (14a)$$

$$\text{Im}(\omega_{ia}) = -\sqrt{\frac{\pi}{8}} \frac{\text{Re}(\omega_{ia})}{(1 + k_{ia}^2 \lambda_D^2)^{3/2}} \left\{ \left(\frac{T_e}{T_i} \right)^{3/2} \exp\left(-\frac{T_e}{2T_i(1 + k_{ie}^2 \lambda_D^2)}\right) + \sqrt{\frac{m_e}{m_i}} \left(1 - \frac{V_{\text{drift}}}{c_s} \sqrt{1 + k_{ia}^2 \lambda_D^2}\right) \right\}, \quad (14b)$$

where k_{ia} is the longitudinal wave number, parallel to V_{drift} by definition; c_s is the sound speed; and λ_D the Debye length defined as

$$\lambda_D = \frac{\sqrt{K_B T_e / m_e}}{2\pi f_{pe}}, \quad \text{i.e., } 69 \sqrt{\frac{T_e}{n_e}} \quad \text{in SI units}, \quad (15)$$

where f_{pe} is the electron plasma frequency. The threshold of the ion-acoustic instability is when the second term inside the large braces in equation (14b) balances the exponential term (Landau damping), so as $\text{Im}(\omega_{ia})$ becomes positive. Everywhere within the highlighted domain shown in Figure 6, the condition $c_s > 100$ m/s is fulfilled. Then, applying equation (14a) to any frequency smaller than 70 Hz, yields a wave number $k_{ia} \leq 4.4 \text{ m}^{-1}$. With $n_e \geq 4.10^8 \text{ m}^{-3}$ and $T_e \leq 1000 \text{ K}$ (Figure 6), the Debye length is nowhere larger than 11 cm; then, the condition $k_{ia}^2 \lambda_D^2 \ll 0.23$ is fulfilled. As long as the condition for the critical drift velocity is also fulfilled ($V_{\text{drift}} > c_s$), not only equation (14b) simplifies but one can make use of the cold plasma approximation by neglecting the Landau damping term in favor of a growing instability. Then, the instability growth rate (γ) obeys the approximate expression

$$\gamma = \frac{\text{Im}(\omega_{ia})}{\text{Re}(\omega_{ia})} \approx \sqrt{\frac{\pi m_e}{8 m_i}} \left(\frac{V_{\text{drift}}}{c_s} - 1 \right) > 0. \quad (16)$$

The first return of this result is that the ion-acoustic instability, triggered by longitudinal sheets of Pedersen currents, is unlikely to exist below ~ 1000 km in the sunlight hemisphere under ramside conditions of Titan-Saturn's magnetosphere interaction. Moreover, substituting the most likely values of n_e and m_i in equation (11), it appears that nowhere the ion-plasma frequency could be lower than about 440 Hz between 1200 and 900 km. Thus, the absence of any SR mode higher than the second one observed at around of 36 Hz during Huygens descent cannot be explained by the ion-acoustic cutoff at the ion-plasma frequency. An alternative explanation is then proposed in the next section, namely, a coupling mechanism between the ELF electric field components of both electrostatic ion-acoustic and electromagnetic quasi-transverse whistler modes.

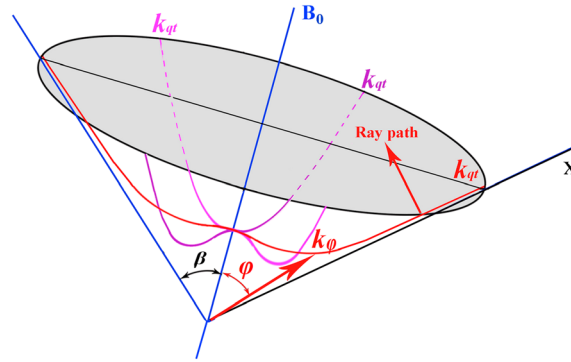


Figure 7. Polar plot of the surface wave vector in the quasi-transverse whistler mode versus the angle ϕ around \mathbf{B}_0 . Note that the wave is circularly polarized, and the energy is propagating globally along the magnetic field lines (not to scale).

4. Coupling Mechanism Between Ion-Acoustic Turbulence and Whistler Mode

The coupling between ion-acoustic and whistler mode waves has been put forward as a mechanism contributing to the dynamics of the upstream region of the Earth's bow shock [Orlowski *et al.*, 1995] involving nonlinear processes due to the presence a bi-Maxwellian electron distribution [Rao and Shukla, 1998]. This mechanism was also evoked as one of possible sources of a presumed Titan's Schumann resonance after preliminary analyses of Huygens PWA data [Béghin *et al.*, 2007]. However, besides the raising interest

in stimulating ELF-VLF emissions by HF heating in the Earth's *D* region [e.g., Papadopoulos *et al.*, 2003], no experimental evidence is known to date about a natural self-modulation of the electrojets in the auroral regions. Nevertheless, the most relevant experiments of HF heating regarding the excitation mechanism of terrestrial SRs, successfully performed in the frequency range of the terrestrial SRs (e.g., Mc Carrick *et al.* [1990], and many other afterward), give us some inputs for understanding the coupling mechanism between electrostatic (ES) and electromagnetic (EM) waves. This mechanism seems indeed to be the most convenient way for radiating a significant fraction of electromagnetic energy away from the current sheets of the ionopause region to feed the Schumann cavity. Thus, the first parameter to be estimated now is the range of relevant ELF frequencies being constrained by our model of Titan's ionopause region.

4.1. Probable ELF Frequency Range of Coupled Ion-Acoustic and Whistler Modes

The dispersion relation of the quasi-transverse whistler mode in a cold, magnetized, and weakly collisional plasma [Booker, 1984] reads

$$k_\phi = \frac{2\pi f}{c} \left(1 + \frac{f_{pe}^2/f^2}{f_{ce} \cos \phi / f - 1 + iv/2\pi f} \right)^{1/2}, \quad (17)$$

where k_ϕ is the amplitude of the complex wave vector making an angle ϕ with respect to \mathbf{B}_0 for any frequency larger than the collision rate and smaller than the electron cyclotron frequency defined as

$$f_{ce} = \frac{q_e B_0}{2\pi m_e}. \quad (18)$$

The collision rate applicable to the whistler mode at frequencies much lower than f_{ce} is assumed to be of elastic nature between thermal electrons and nitrogen neutral molecules, the expression of which derived by Banks and Kockarts [1973] reads

$$\nu = \nu_{en} = 2.33 \times 10^{-17} T_e n_n \text{ (SI units)}. \quad (19)$$

When ϕ tends toward the so-called resonance cone of half-angle β defined as $\text{Arcos}(f/f_{ce})$, it is straightforward from equation (17) that k_ϕ tends to very large values (Figure 7), approaching the same order of magnitude as the ion-acoustic wave vector k_{ia} . Applying to equations (13)–(16) the coupling condition satisfying the mutual equality between the frequencies and the wave vectors components of both modes, one obtains the following dispersion equation of the common frequency f_{qt}

$$f_{qt}^2 - f_{qt} f_{ce} \cos \beta + f_p^2 c_s^2 / c^2 = 0, \quad (20)$$

where the collision frequencies are neglected as long as the condition $f_{qt} > \nu/2\pi$ holds. Because the last left-hand term of equation (20) is several orders of magnitude smaller than the other terms, the solution for f_{qt} is

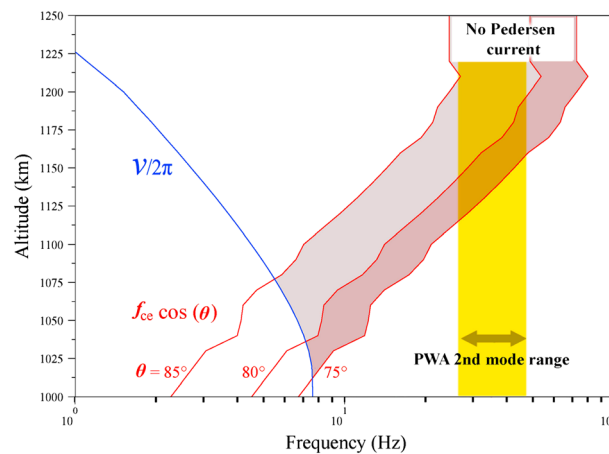


Figure 8. Permitted ranges of coupled ES-EM waves for $85^\circ < \beta < 75^\circ$, using the altitude profiles plotted in Figures 5 and 6.

interaction presumed to be those occurring during the Huygens descent. However, nothing allows considering this situation as a nominal case; then, for different conditions several SR modes could have been observed, or even none at all, on January 2005.

4.2. Mechanism of ELF Current Modulation

The last item to be studied is the physical mechanism of ELF modulation of the current sheets. In the previous section, the coupling conditions between the longitudinal wave vectors of the ion-acoustic and the quasi-transverse whistler modes allowed us to define the frequency range in which the energy transfer mechanism is made possible. But this does not explain by which means the sheet currents \mathbf{J} are modulated in that frequency range.

Referring to Earth's experiments of polar ionosphere HF heating (e.g., *Stubbe and Koppa* [1977] and *Mc Carrick et al.* [1990], and several others), the Titan's conditions are different because of the following:

1. The Earth's current sheets exist naturally on form of auroral electrojets that are able to generate different kinds of plasma instabilities, except the spontaneous emission of natural ELF/VLF electromagnetic wave emissions. The reason is because the natural Pedersen conductivity is generally too weak to meet the coupling conditions.
2. However, a powerful HF wave emitted from the ground, with a given ELF-VLF modulation, allows the conductivity to grow up to a critical threshold owing to the electron heating, so as to trigger the ion-acoustic instability in the presence of electrojet. Then, the ELF-VLF wave emission process becomes possible as long as the coupling conditions defined in the previous section are fulfilled. An electromagnetic mode can be received at the ground with the modulation frequency of the HF pump, although it has been reported that signals at higher order harmonics might be observed [e.g., *Mc Carrick et al.*, 1990].

In spite of many theoretical and experimental works, several aspects of such nonlinear modulation mechanisms of these heating experiments remain unresolved [*Papadopoulos et al.*, 2003]. Nevertheless, an explanation of the modulation mechanism of current sheets in the Earth's polar electrojet, forced by HF heating, has been proposed by *Kuo et al.* [1999] to be the source of stimulated whistler waves propagating downward. In the case of Titan, the natural conductivity is shown in section 3 to be able to overpass by itself the threshold of current-driven instability (Figure 6). Then, the basic mechanism proposed by *Kuo et al.* [1999] should apply in our case. According to these authors, the modulated current sheets are acting as a current antenna, which is exactly what is needed to excite the Schumann tesseral LSM modes [*Béghin et al.*, 2012]. It is worth to note that contrary to Earth's heating experiments aiming to trigger a backward propagation of a whistler emission through the lower ionosphere, we are rather concerned here with the modulation mechanism of current sheets that are actually the sources of Titan's Schumann resonances (Figure 1).

In the vicinity of the resonance cone, the electric field and the \mathbf{k} vector are aligned [*Stix*, 1962], and the wave is quasi-static, with the raypath (Poynting vector) nearly parallel to \mathbf{B}_0 when β is large (Figure 7), which is

very close to the local value of the oblique resonance frequency $f_{ce} \cos \beta$, where β is the dip angle between \mathbf{B}_0 and the relevant current sheet J_x (Figure 1). The permitted range of frequencies plotted in Figure 8 is obtained using the ionopause parameters of our model and assuming the values of the dip angle β lying between 75° and 85° . The latter values are selected so as to demarcate the favorable conditions for the presence of the second SR eigenmode only, as seen in the PWA data at around 35–36 Hz (Figures 2 and 3). It must be emphasized indeed that the purpose of this simulation is to show that the absence of higher modes in PWA data can be explained by the physical conditions of Titan-Saturn's magnetosphere

precisely the case shown in Figure 1. The coupling mechanism of both modes along the x axis brings us to consider the following condition applied to the electric field component E_x which is common to both modes:

$$E_x = E_0 + \Sigma_k \delta_{qt} \exp[i(\omega_{qt}t - \mathbf{k} \cdot \mathbf{x})] \quad (21)$$

where E_0 is the constant component that drives the electron drift velocity along the longitudinal axis. The last term is the Fourier spectral amplitude of the ELF elementary components δ_{qt} of the whistler electric field projected along the x axis, according to the principle invoked by Kuo *et al.* [1999]. The electric field components of the traveling waves along the x axis, represented by the second term of equation (21), are now acting as a feedback modulator of the Pedersen currents, such as

$$J'_x = J_x + \sigma_p \Sigma_k \delta_{qt} \exp[i(\omega_{qt}t - \mathbf{k} \cdot \mathbf{x})], \quad (22)$$

where J'_x is the time-varying amplitude of the ELF-modulated current and J_x its parent DC value. The efficiency of the current modulation is determined by the growth rate γ of the ion-acoustic instability in the relevant region (Figure 6) and the excited frequency range (Figure 8). Thus, each portion of modulated Pedersen current sheets is acting as an antenna able to radiate the most excited frequencies seen in the PWA data (Figures 2 and 3), provided that β in the source region was lying between 75° and 85° during the Huygens descent (Figure 1). Such values of β are indeed compatible with a bipolar configuration, and the frequency range accounts for the observation of a dominating second SR eigenmode excited by current sheets lying at around 1100–1200 km (Figure 6).

5. Summary and Conclusion

The analytical spectral distributions of Schumann resonance eigenmodes are computed from the modal equation derived in previous works from the ELF PWA data of the Huygens Probe and considering the most likely constrained parameters of the ramside atmospheric cavity during the descent. Two case study simulations are performed considering different sets of parameters for the cavity. Each simulation is made successively in two steps: the first one ignoring the instrumental noise contribution and the second step including the noise. The case study # 1 involves the combination of the two first eigenmodes, and the same operation is performed for the second and third modes in the case study # 2. The comparison between the combined spectral responses and the Huygens PWA data leads to conclude that the presence of the fundamental mode had, respectively, 50% and 25% of chance to be visible in 24 and 18 Hz bins. In either case study, the simulated spectral density of the second mode fits satisfactorily the experimental data between 30 and 42 Hz, whereas an extremely weak signature of the third mode between 42 and 60 Hz cannot be excluded. Thus, one may conclude that the generation mechanism of Titan's Schumann resonances must imply a narrow band filter associated with the peculiarities of the source and a central frequency lying at around 36 Hz that corresponds to the presumed second SR mode in the particular conditions of Huygens descent.

By the mere fact that the generation mechanism by lightning activity in Titan's atmosphere is most unlikely, in spite of many attempts to detect such events, an alternative atypical generation mechanism is proposed. The latter involves a primary source of energy, namely, the ELF ion-acoustic turbulence induced in the ionopause region by the electron-ion drift velocity associated with the Titan-Saturn's magnetosphere interaction. A secondary process involves the modulation of the induced longitudinal Pedersen current sheets, fitting together the ranges of frequencies and wave vectors, respectively, of both ion-acoustic and quasi-transverse whistler modes. This work is a rational attempt to explain and conciliate two unexpected experimental facts. First, how a Schumann resonance in Titan's ionosphere in the absence of lightning activity might exist? Second, why the sole second Schumann eigenmode was observed during the Huygens descent? The common answer to both questions is closely associated with the generation mechanism that implies in itself a narrow band filtering, which is not the case with the Earth's lightning sources. Such scenario of Schumann resonance emission is presumably unique in the solar system because it needs, at once, the presence of a significant ionized atmosphere, a ground or buried conductive surface, and some identified source of energy in the absence of lightning activity; all three conditions known to date to be solely applicable to Titan. As an ultimate recommendation addressed to the designers of future missions to Titan, I would like to point out the greatest interest to reiterate the pioneer measurements of electromagnetic fields in Titan's atmosphere performed with the Huygens Probe. By extending the exploration frequency range of both electric and magnetic field components from DC to VLF, it is expected not only to confirm definitely the existence of a Titan's Schumann resonance and a buried water ocean but also to improve the knowledge of their physical properties.

Acknowledgments

The author is grateful to LPC2E institute and his director Dr. Michel Tagger, for the support provided him as an emeritus scientist, and wishes to acknowledge his near colleagues of the PWA team for several years of lasting joint cooperation. Warm attention is paid to Dr. L.R.O. Storey for his always pertinent comments and to this work in particular.

References

- Ågren, K., et al. (2011), Detection of currents and associated electric fields in Titan's ionosphere from Cassini data, *J. Geophys. Res.*, **116**, A04313, doi:10.1029/2010JA016100.
- Alexandrov, A. F., L. S. Bogdankevich, and A. A. Rukhadze (1984), *Principles of Plasma Electrodynamics*, pp. 488, Springer, New York.
- Baker, W. G., and D. F. Martyn (1953), Electric currents in the ionosphere. I. The conductivity, *Phil. Trans., R. Soc. London, Ser. A Math. Phys. Sci.*, **246**(913), 281–294.
- Banks, P. M., and G. Kockarts (1973), *Aeronomy*, Academic Press, New York and London.
- Batman, H. (1954), *Tables of Integral Functions*, vol. 1, pp. 392, McGraw-Hill Book Company, Inc, New York, Toronto, London.
- Béghin, C., et al. (2007), A Schumann-like resonance on Titan driven by Saturn's magnetosphere possibly revealed by the Huygens Probe, *Icarus*, **191**, 251–266.
- Béghin, C., et al. (2009), New insights on Titan's plasma-driven Schumann resonance inferred from Huygens and Cassini data, *Planet. Space Sci.*, **57**, 1872–1888.
- Béghin, C., M. Hamelin, and C. Sotin (2010), Titan's native ocean revealed beneath some 45 km of ice by a Schumann-like resonance, *C. R. Geosci.*, **342**, 425–433.
- Béghin, C., et al. (2012), Analytic theory of Titan's Schumann resonance: Constraints on ionospheric conductivity and buried water ocean, *Icarus*, **218**, 1028–1042.
- Booker, H. G. (1984), *Cold Plasma Waves*, pp. 1–345, Martinus Nijhoff Pub, Dordrecht, Boston, Lancaster.
- Collin, R. (1991), *Field Theory of Guided Waves*, 2nd ed., pp. 852, IEEE Inc. Press, New York.
- Crary, F. J., B. A. MaGee, K. E. Mandt, J. H. Waite, J. Westlake, and D. T. Young (2009), Heavy ions, temperatures and winds in Titan's ionosphere: Combined Cassini CAPS and INMS observations, *Planet. Space Sci.*, **57**, 1847–1856.
- Cui, J., et al. (2009), Analysis of Titan's neutral upper atmosphere from Cassini Ion Neutral Mass Spectrometer measurements, *Icarus*, **200**, 581–615.
- Eddberg, N. J. T., J.-E. Wahlund, K. Ågren, M. W. Morooka, R. Modolo, C. Bertucci, and M. K. Dougherty (2010), Electron density and temperature measurements in the cold plasma environment of Titan: Implication for atmospheric escape, *Geophys. Res. Lett.*, **37**, L20105, doi:10.1029/2010GL044544.
- Fischer, G., and D. A. Gurnett (2011), The search for Titan lightning radio emissions, *Geophys. Res. Lett.*, **38**, L08206, doi:10.1029/2011GL047316.
- Fulchignoni, M., et al. (2005), In situ measurements of the physical characteristics of Titan's environment, *Nature*, **438**(8), doi:10.1038/nature04314.
- Galand, M., R. V. Yelle, A. J. Coates, H. Backes, and J.-E. Wahlund (2006), Electron temperature of Titan's sunlit ionosphere, *Geophys. Res. Lett.*, **33**, L21101, doi:10.1029/2006GL027488.
- Galejs, J. (1972), *Terrestrial Propagation of Long Electromagnetic Waves*, 362 pp., Pergamon Press, Oxford, New York, Toronto, Sydney.
- Grard, R., et al. (2006), Electric properties and related physical characteristics of the atmosphere and surface of Titan. *Planet. Space Sci.*, **54**, 1124–1136.
- Gurnett, D. A., et al. (2004), The Cassini radio and plasma wave investigation, *Space Sci. Rev.*, **114**, 395–463.
- Keller, C. N., T. E. Cravens, and L. Gan (1994), One-dimensional multispecies magnetohydrodynamic models of the ramside ionosphere of Titan, *J. Geophys. Res.*, **99**(A4), 6511–6525.
- Kliore, A. J., et al. (2008), First results from the Cassini radio occultations of the Titan ionosphere, *J. Geophys. Res.*, **113**, A09317, doi:10.1029/2007JA012965.
- Kuo, S. P., E. Koretzky, and M. C. Lee (1999), A new mechanism of whistler generation by amplitude modulated HF waves in the polar electrojet, *Geophys. Res. Lett.*, **26**(12), 1677–1680.
- Leach, W., Jr. (1994), Fundamentals of low-noise electronics. *Proc. IEEE*, **82**(10), 1515–1538.
- McCarrick, M. J., D. D. Sentman, A. Y. Wong, R. F. Wuerker, and B. Chouinard (1990), Excitation of ELF waves in the Schumann resonance range by modulated HF heating of the polar electrojet, *Radio Sci.*, **25**(6), 1291–1298.
- Neubauer, F. M., et al. (2006), Titan's near magnetotail from magnetic field and electron plasma observations and modeling: Cassini flybys TA, TB, and T3, *J. Geophys. Res.*, **111**, A10220, doi:10.1029/2006JA011676.
- Nickolaenko, A. P., and D. D. Sentman (2007), Line splitting in the Schumann resonance oscillations, *Radio Sci.*, **42**, RS2513, doi:10.1029/2006RS003473.
- Orlowski, D. S., C. T. Russell, D. Krauss-Varban, N. Omid, and M. F. Thomsen (1995), Damping and spectral formation of upstream whistlers, *J. Geophys. Res.*, **100**, 17,117, doi:10.1029/95JA00062.
- Papadopoulos, K., T. Wallace, M. McCarrick, G. M. Milikh, and X. Yang (2003), On the efficiency of ELF/VLF generation using HF heating of the auroral electrojet, *Plasma Phys. Rep.*, **29**–7, 561–565.
- Rao, N. N., and P. K. Shukla (1998), Coupled whistler and ion-acoustic mode propagation in two-electron-temperature plasmas, *Phys. Lett. A*, **243**, 151–155.
- Rosenberg, M., and P. K. Shukla (2009), On the possibility of ion-acoustic instability in Titan's ionosphere, *Planet. Space Sci.*, **57**, 2030–2031.
- Rosenqvist, L., J.-E. Wahlund, K. Ågren, R. Modolo, H. J. Opgenoorth, D. Strobel, I. Müller-Wodarg, P. Garnier, and C. Bertucci (2009), Titan ionospheric conductivities from Cassini measurements, *Planet. Space Sci.*, **57**, 1828–1833.
- Simões, F., et al. (2007), A new numerical model for the simulation of ELF wave propagation and the computation of eigenmodes in the atmosphere of Titan: Did Huygens observe any Schumann resonance?, *Planet. Space Sci.*, **55**, 1978–1989.
- Simon, S., S. C. van Treeck, A. Wennmacher, J. Saur, F. M. Neubauer, C. L. Bertucci, and M. K. Dougherty (2013), Structure of Titan's induced magnetosphere under varying background magnetic field conditions: Survey of Cassini magnetometer data from flybys TA-T85, *J. Geophys. Res. Space Physics*, **118**, 1679–1699, doi: 10.1002/jgra.50096, in press.
- Stix, T. H. (1962), *The Theory of Plasma Waves*, vol. 283, McGraw-Hill, New York.
- Stubbe, P., and H. Koppe (1977), Modulation of the polar electrojet by powerful HF waves, *J. Geophys. Res.*, **82**(16), 2319–2325.
- Wahlund, J.-E., et al. (2009), On the amount of heavy molecular ions in Titan's ionosphere, *Planet. Space Sci.*, **57**, 1857–1865.
- Wait, J. R. (1962), *Electromagnetic Waves in Stratified Media*, p. 372, Pergamon Press, Oxford, London, New York, Paris.